The chemical dynamics of the reactions of O(3 P) with saturated hydrocarbons. I. Experiment

P. Andresen and A. C. Luntz

Citation: The Journal of Chemical Physics **72**, 5842 (1980); doi: 10.1063/1.439108
View online: http://dx.doi.org/10.1063/1.439108
View Table of Contents: http://scitation.aip.org/content/aip/journal/jcp/72/11?ver=pdfcov
Published by the AIP Publishing

The chemical dynamics of the reactions of $O(^3P)$ with saturated hydrocarbons. I. Experiment

P. Andresen[a] and A. C. Luntz

IBM Research Laboratory, San Jose, California 95193
(Received 28 December 1979; accepted 22 February 1980)

Molecular beam-laser induced fluorescence experiments have probed the nascent internal state distributions and excitation functions of OH formed in the technologically important reactions $O(^3P) + RH \rightarrow OH + R\cdot$. RH is a saturated hydrocarbon and R· is an alkyl radical. A variety of RH have been investigated corresponding to abstraction of primary, secondary, and tertiary hydrogens. The OH rotational state distribution is nearly identical for all RH and decrease rapidly from its peak at the lowest rotational level. This demonstrates that reaction occurs when $O(^3P)$ is collinear to a C–H bond in the hydrocarbons. The vibrational state distribution of OH depends markedly on the type of hydrogen abstracted, with vibrational excitation increasing dramatically across the series primary to secondary to tertiary. This is interpreted as a shift from a repulsive towards a more attractive surface across the series. Partitioning into the OH spin doublets shows that these reactions are midway between the adiabatic and diabatic limits with respect to the spin–orbit surfaces. Excitation functions measure the dynamic thresholds, and are in good agreement with activation energies obtained from thermal rate constants. The excitation functions for $v = 1$ OH exhibit a sharp decrease at energies considerably above threshold. This suggests that excitation of internal modes of R· occurs only at high collisions energies. All of these results are interpreted qualitatively in terms of a simple, but general, triatomic model for the interaction of $O(^3P)$ with RH, i.e., where R· can be considered a structureless particle.

I. INTRODUCTION

The reactions of the electronic ground state of the oxygen atom $O(^3P)$ with organic hydrocarbons play a central role in many important chemical environments, e.g., combustion, air pollution, and atmospheric chemistry. Because of this, there have been literally hundreds of measurements of thermal rate constants for these reactions for use in kinetic models.[1] To date, however, no detailed chemical dynamics information is available for these technologically important reactions. Thus, few qualitative, and no quantitative, features of the chemical interactions are known.

The mechanism that is generally assumed for the reaction of $O(^3P)$ with saturated hydrocarbons RH is a simple hydrogen abstraction, i.e.,

$$O(^3P) + RH \rightarrow OH + R\cdot , \qquad (1)$$

where R· is an alkyl radical. Although no direct evidence proves that this mechanism dominates the chemistry, indirect experiments[2] and quantum chemical arguments[3] suggest this pathway.

For $O(^3P)$ abstraction in saturated hydrocarbons, it is necessary to distinguish three types of C–H bonds: primary (RCH_3), secondary (R_2CH_2), and tertiary (R_3CH). R is some other radical species and represents a C–C bond. This classification is necessary because the various C–H bonds have different bond strengths, i.e., ~100, ~95, and ~92 kcal/mole for primary, secondary, and tertiary bonds, respectively.[4] This produces both different reaction energetics and kinetics in the three cases. The results are summarized in the correlation diagrams of Fig. 1, which are schematic one dimensional representations of the potential energy surfaces for abstraction in each case. In this figure, the energetics of the asymptotic reactant and product states are given by thermodynamics, while the interaction regions are estimated from activation energies obtained from thermal rate constant measurements.[5] All reactions are slightly exothermic with $\Delta H = -2.3$, -7.0, and -10.3 kcal/mole for primary, secondary, and tertiary abstraction, respectively. The barriers to re-

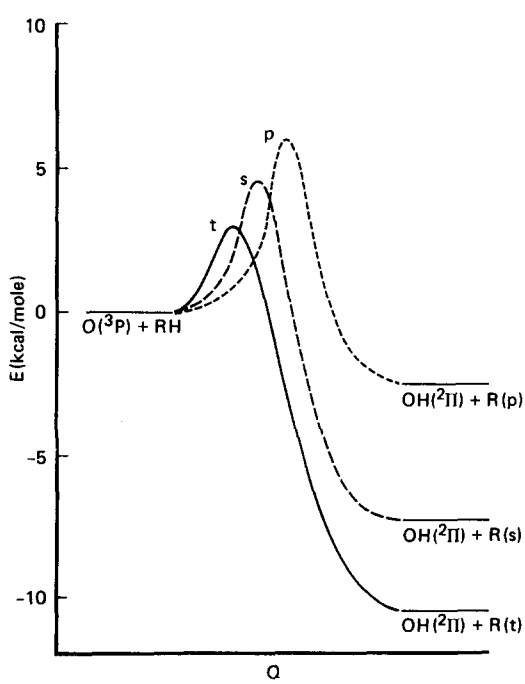

FIG. 1. Schematic correlation diagrams for the reactions of $O(^3P)$ with saturated hydrocarbons. E is the energy and Q is the reaction coordinate. The curves are labeled P, S, and T to represent abstraction of primary, secondary, and tertiary hydrogens, respectively.

[a] Permanent address: Max-Planck Institut für Strömungsforschung, 34 Göttingen, Böttingerstrasse 6-8, West Germany.

 0021-9606/80/115842-09$01.00

action vary substantially in the series and are ~6.9, ~4.5, and ~3.3 kcal/mole, respectively. For reference in later discussions, we note that the $OH(v=1)$ state is located 10 kcal/mole above the asymptotic product levels of Fig. 1.

Although rate constant measurements do not directly reveal the detailed reaction dynamics, they do suggest some generalities. The thermal rates for $O(^3P)+RH$ reactions are quite slow. This is due not only to the presence of appreciable activation energies, but also to somewhat small pre-exponential factors in the Arrhenius form of the rate constant.[5] These pre-exponential factors, typically ~10%–20% of those predicted from gas kinetic cross sections imply that there must exist some selective steric requirement for reaction. Activation energies and pre-exponential factors per C–H bond do depend significantly on the type of C–H bond abstracted, but are otherwise rather independent of the exact nature or complexity of the hydrocarbon reactant. Thus, rates for large complex hydrocarbons are approximately predicted as the sum of the rates of the individual C–H bonds.[5] This bond additivity in rates and the abstraction mechanism both suggest that the reaction involves strong interaction of $O(^3P)$ with only the individual C–H bonds, rather than with the entire hydrocarbon molecule simultaneously.

Detailed dynamical information on the reactions can be obtained from the nascent internal state distribution of the products, e.g., $OH(v,K,f)$, where v is the vibrational quantum number, K is the rotational quantum number, and f refers to one of the four OH fine structure levels. It is well known that such distributions reflect the history of the reactive collision and therefore can probe the intermolecular potential surface.[6] For example, in many exothermic reactions, rotational excitation of the product results from the torque imparted to the fragment as the original bond breaks.[7] Thus, the product rotational distribution can yield considerable information on the geometry of the transition state. Extensive classical scattering calculations on model potential surfaces by Polanyi and co-workers[8] show that vibrational state distributions in the products are sensitive to where the original bond breaks along the reaction coordinate, i.e., the location within the reactive potential surface of the point of steepest descent. The dependence of these state distributions and of the individual reactive cross sections on the initial collision energy provide many further details of the dynamics and surfaces.

Since the $O(^3P)+RH$ reactions are slow thermal reactions even at elevated temperatures, the nascent product state distributions can only be measured in molecular beam experiments under single collision conditions. Otherwise, the measured distributions would be severely distorted by faster relaxation processes. In addition, it is necessary to surmount the energy barrier to reaction to obtain significant reactive cross sections. This is possible in molecular beam experiments since the initial collision energy between the reactants can be substantially increased and controlled through the beam velocities.

We report here the first measurements of the nascent OH product state distributions for the reaction of $O(^3P)$ with several saturated hydrocarbons under crossed molecular beam conditions. These experiments use the technique of laser induced fluorescence[9] to detect the product OH. The initial collisional energy dependence of the state distributions and individual reactive cross sections are also reported. These results confirm the abstraction mechanism and provide detailed information on the dynamics and reactive potential surfaces. Comparison of the results for different hydrocarbons suggests a very general but simple triatomic model which qualitatively describes the dynamics and intermolecular interactions for all $O(^3P)+RH$ reactions. The following paper[13] presents a quantitative comparison of this model with the experimental results presented in this paper.

II. EXPERIMENTAL

Nascent OH internal state distributions and excitation functions for the reactions $O(^3P)+RH\rightarrow OH+R\cdot$ have been measured using crossed molecular beam scattering with laser induced fluorescence (LIF) detection of the OH product in a manner similar to that described previously.[11] The detection of OH is accomplished by irradiating the scattering zone of the two reactant beams with a tunable pulsed UV laser. The total fluorescence is measured as the laser is scanned through the $^2\Sigma\leftarrow{}^2\Pi$ absorption band of OH.[10] The internal state distributions are obtained by converting the relative intensities of this excitation spectrum to OH state densities using the known radiative properties of OH.[11,12] Relative cross sections for each OH state are obtained by converting these densities to fluxes through

$$\sigma_{OH}(i)\sim\frac{n_{OH}(i)}{n_0 n_{RH}\langle g/v_{OH}(i)\rangle}R\ . \tag{2}$$

$\sigma_{OH}(i)$ is the cross section into the ith internal level; $n_{OH}(i)$, n_0, and n_{RH} are the respective densities; g is the magnitude of the initial relative velocity vector in the center of mass coordinate system; $v_{OH}(i)$ is the magnitude of the final velocity of OH in the ith level in the laboratory coordinate system; and the $\langle\ \rangle$ denotes averaging over all scattering angles and initial beam conditions. R is the effective radius of the scattering volume. Since only the scattering zone is probed by the laser, integral cross sections are obtained in these experiments.

In principle, the flux–density transformation $\langle g/v_{OH}(i)\rangle$ can depend on the angular distribution of scattering and on the fraction of the total reaction energy partitioned into internal modes of $R\cdot$, both of which have not been measured. The classical scattering calculations on the model potential surfaces that are reported in the following paper[13] show that the OH angular distribution is peaked backwards relative to $O(^3P)$ in the center of mass system. Fortunately, for our experimental beam velocities, the flux–density transformation is then dominated by the velocity of the center of mass motion rather than the recoil velocity of OH in the center of mass system. In this case, the transformation is rather insensitive to the exact form of the angular scattering and to the fraction of total energy deposited into $R\cdot$ vibrational modes. Since only relative cross sections are obtained

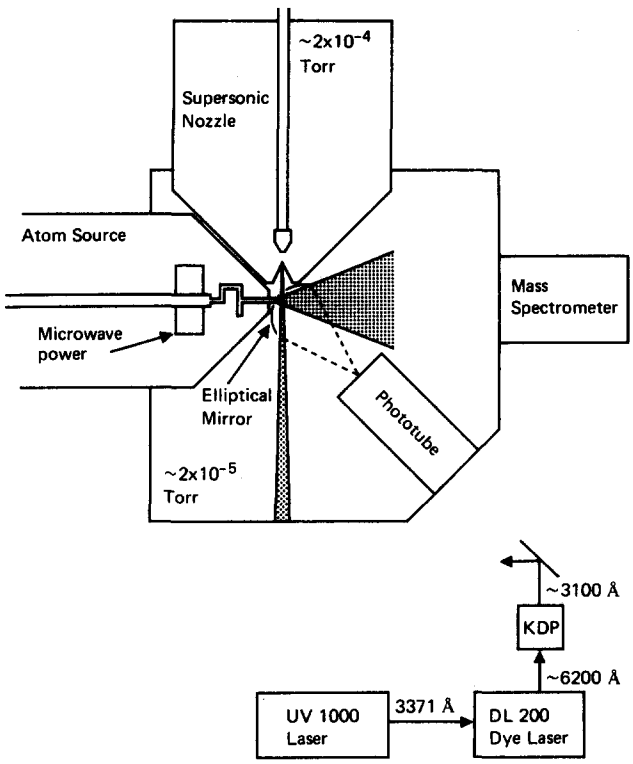

FIG. 2. Schematic diagram of the molecular beam–laser induced fluorescence experiment.

in these experiments, only ratios of $\langle g/v_{OH}(i)\rangle$ are required. These are even less sensitive to the unmeasured distributions. Uncertainties in relative values of $\langle g/v_{OH}(i)\rangle$ are $\leq 10\%$ for all center of mass angular distributions between sharp backward scattering and isotropic scattering. Uncertainties in relative $\langle g/v_{OH}(i)\rangle$ are also $\leq 15\%$ for anywhere from 0% to 50% of the total energy partitioned into modes of R·. Actual values of $\langle g/v_{OH}(i)\rangle$ used throughout this paper are calculated assuming a 45° HWHM scattering distribution centered in the backward direction and none of the reaction energy partitioned into internal modes of R·.

A schematic diagram of the experiment is given in Fig. 2. Since many aspects of this experiment have been presented previously,[11] only modifications and procedures necessary for the results reported here are described.

The O(^3P) beam source is based on well known discharge flow techniques. The atoms are generated by a microwave discharge in O_2 at a pressure of ~0.3 Torr. Following the discharge, the atoms flow through a 10 cm length of 3 mm tubing and expand directly into the scattering chamber. The flow tube contains several 90° bends terminated by Wood's horns and is externally painted black in order to block light generated in the discharge from entering the scattering chamber. Flow of atoms along this tube also translationally cools the atoms formed in the discharge and quenches other reactive species, e.g., O($^1D_2$). $O_2(^1\Delta)$ is probably present in the beam,[14] but is not reactive with saturated hydrocarbons. Approximately 3% H_2O is added to the O_2 flow to increase the dissociation efficiency,[15] and the walls of the flow tube are coated with boric acid to inhibit heterogeneous recombination.[16] Typically, ~25% dissociation efficiency is achieved as shown by the decrease in O_2 beam flux when the discharge is turned on. The beam flux is measured by modulated beam mass spectrometry. The end of the flow tube is 0.7 cm from the scattering center. The overall atom source acts as a single long capillary effusive source. It provides a broadly divergent beam of ~40° FWHM with a thermal velocity distribution of ~340°K as measured by time of flight experiments. The O and O_2 fluxes from this source generate a background pressure in the scattering chamber of $\sim 3\times10^{-5}$ Torr.

A translationally accelerated RH reactant is generated by a seeded nozzle beam[17] containing 2%–35% RH in either H_2 or He as the carrier gas. The nozzles are operated at ~3800 Torr stagnation pressures and expand through a 50 μm nozzle hole. A skimmer with a 0.8 mm diameter orifice collimates the beam to 3° HWHM. As measured by TOF, Mach numbers for RH were ≥ 25 and no slip of the RH velocity relative to that of the carrier gas was observed. The translational energy of RH is controlled by varying the percentage of RH in the carrier gas, changing the carrier gas, and by heating of the nozzle tip. Overall, the average center of mass collision energy E_c is varied over the range of 2–17 kcal/mole.

Time of flights are measured using a step function chopper and a mass spectrometer as the beam detector. The output is monitored by a Biomation 610 transient recorder which is connected to an IBM System/7 computer for averaging of many chopper cycles. Velocities are determined from the additional flight time when a 1 m differentially pumped tube is inserted in the beam flight path. Resolution in the flight time is typically 2% and this produces an uncertainty in the average collision energy of ~5%.

Since H_2O is added to the O(^3P) beam source to enhance dissociation, a large background of OH in $v=0$ and with a ~300°K Boltzmann distribution of rotational states is present in the scattering center. To distinguish this background from reactive scattering into these states, the RH beam is modulated. This is accomplished by placing a fast shutter of 1 mm width in front of the skimmer opening. The shutter is driven by a Uniblitz LR12 fast solenoid valve modified for effective heat dissipation in vacuum. The shutter is opened for ~3 msec only every other laser pulse, so that LIF is measured both with and without the RH beam, and the difference signal is obtained. The reactive signal in $v=0$ is only 10%–20% of the background and this limits S/N for reactive scattering into low rotational states of $v=0$.

The entire experiment is coupled on line to an IBM System/7 computer for effective time averaging. Laser wavelength, laser firing, the fast beam shutter, and data acquisition are controlled by the computer.

To insure that the measurements were not distorted by collisional relaxation, the O(^3P) beam flux, and hence the background pressure in the scattering chamber, was reduced in stages by one order of magnitude. The mea-

sured state distribution was independent of this variation, while each reactive signal intensity was strictly linear with the $O(^3P)$ flux. Both guarantee the single collision limit.

A variety of different hydrocarbons have been investigated as the reactant RH. Principal examples are neopentane $[C(CH_3)_4]$ for abstraction of primary hydrogens, cyclohexane (C_6H_{12}) for secondary hydrogens, and isobutane $[(CH_3)_3CH]$ for tertiary abstraction. The first two have all equivalent primary and secondary hydrogens, respectively, while isobutane contains one tertiary and nine primary hydrogens. It will be shown later that the tertiary site is much more reactive than the primary hydrogens, and thus this molecule serves as a good example of tertiary abstraction. Hexane (C_6H_{14}) has also been investigated as a further example of secondary abstraction. In addition, measurements were performed on the deuterated analogs C_6D_{12} and $(CH_3)_3CD$. Specific experimental procedures used to obtain the excitation functions are presented later.

III. STATE DISTRIBUTIONS OF OH

A. Rotational partitioning

The rotational state distributions in the f_1 fine structure component[10] of OH produced in the reaction $O(^3P) + C_6H_{12} \rightarrow OH + C_6H_{11}$ is presented in Fig. 3. As shown, the maximum reactive cross section is into the lowest rotational level $K=1$ for both the $v=0$ and $v=1$ states of OH, and the cross sections decrease very rapidly with increasing K. The distribution in $v=1$ is even narrower than that in $v=0$. Overall, rotational excitation of OH accounts for only 2% of the total reaction energy.

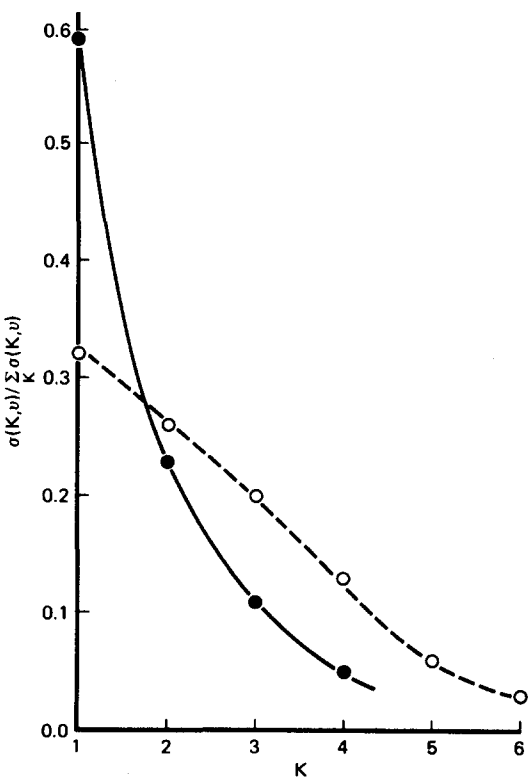

FIG. 3. The normalized rotational state distribution in OH ($v=1$) (●) and OH ($v=0$) (○) produced in the reaction $O(^3P) + C_6H_{12} \rightarrow OH(K,v) + C_6H_{11}$ at $E_c = 7.1$ kcal/mole. K is the rotational quantum number and the ordinate is the relative cross section normalized such that the total scattering into each vibrational state is unity.

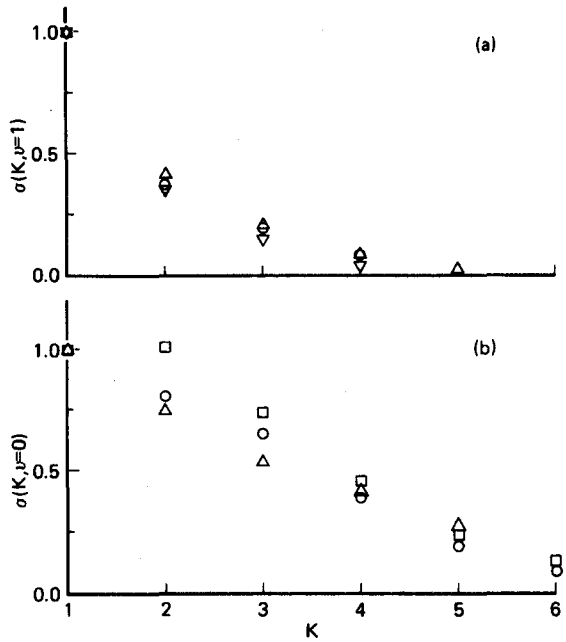

FIG. 4. Comparison of the rotational state distributions obtained with a variety of RH reactants. K is the rotational quantum number and $\sigma(K,v)$ is the relative cross section normalized such that $\sigma(K=1,v)=1$ for each RH: (a) scattering into OH ($v=1$) for C_6H_{12} (○), C_6H_{14}, (△), and $(CH_3)_3CH$ (▽); (b) scattering into OH ($v=0$) for C_6H_{12} (○), C_6H_{14} (△), and $(CH_3)_4C$ (□).

Figure 4 shows the rotational distributions obtained with a variety of very different RH reactants. These reactions correspond to abstraction of primary, secondary, and tertiary hydrogens, as well as abstraction from cyclic or straight chain hydrocarbons. Remarkably, the rotational distributions are nearly identical for all RH reactants. Careful inspection shows that the breadth of the rotational distributions decreases slightly across the series primary to secondary to tertiary abstraction.

Rotational excitation in these reactions arises primarily from the torque imparted to the OH due to repulsion between the product fragments.[7] If reaction occurs principally through bent configurations R–H°, then repulsion in the R–H bond produces a torque in OH and causes substantial rotational excitation. On the other hand, if reaction occurs through collinear intermediates R–H–O, then R–H repulsion produces only translation or vibration of OH with little excitation of rotation. Since only a few of the lowest rotational states are populated in the $O(^3P) + RH$ reactions, they must be dominated by collinear configurations. Although the rotational distribution principally probes the preferred geometry in the exit channel of the reactive surface, similar geometries should dominate the entrance channel as well. Thus, it is inferred that reaction preferentially occurs

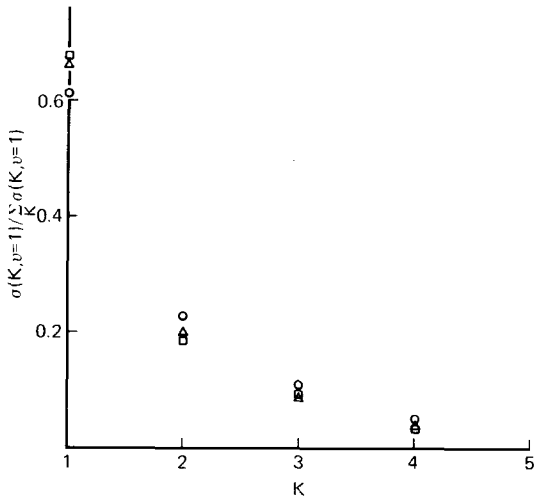

FIG. 5. The effects of E_c, the initial collision energy, on the OH ($v=1$) rotational state distribution in the reaction $O(^3P) + C_6H_{12} \rightarrow OH + C_6H_{11}$. K is the rotational quantum number and the ordinate is the relative cross section normalized such that the total scattering into $v=1$ at each E_c is unity. The values of E_c are 7.1 kcal/mole (○), 6.2 kcal/mole (△), and 4.9 kcal/mole (□).

when $O(^3P)$ approaches collinearly to a C–H bond. This collinear requirement must be quite general for all of the $O(^3P)$ + RH reactions since each produces a similar rotational state distribution. This steric requirement explains the small pre-exponential factors observed in the Arrhenius form of the thermal rate constants.

The dependence of one of the rotational distributions on the initial collision energy E_c is shown in Fig. 5. This rotational distribution is nearly independent of E_c. There is, however, a very slight broadening with E_c. This is also observed in the reaction of $O(^3P) + (CH_3)_3CH$ as well. This minimal broadening of the rotational distribution with E_c also implies that the potential must rise steeply away from the collinear configuration. Otherwise, reactive trajectories could sample increasingly bent configurations as E_c increases. This would result in a substantial broadening of the rotational distribution with E_c.

In addition to product repulsion, both reagent orbital angular momentum L and reactant rotation J_{RH} could contribute to OH rotation. Both are estimated to be quite large, i.e., $\sim 20\hbar$. However, since the collision duration ($\sim 10^{-12}$ sec) is somewhat faster than the rotational period of RH ($\sim 10^{-11}$ sec), J_{RH} should contribute little to OH rotation. In addition, as pointed out by Hijazi *et al.*,[7] transfer of L into product rotation should be minimal for the mass combination involved in the O + RH → OH + R reactions. On the contrary, this mass combination is particularly sensitive to torques generated by product repulsion in bent configurations. Experimentally, the rotational distributions are nearly independent of the velocity of RH and of the nozzle condition, i.e., temperature or whether seeding in H_2 or He. Since J_{RH} and L vary considerably with these changes, this demonstrates that there is almost no conversion of L or J_{RH} into product rotation.

B. Vibrational partitioning

Measurements for OH vibrational partitioning were done by comparing the intensities between $v=0$ and $v=1$ OH for only the $K=1$ rotational ground state. The total cross section into a vibrational state is then obtained by summing over the measured rotational distributions. Table I presents ratios of these total cross sections observed for several RH. Because of the background in $v=0$ OH and the difficulty in comparing LIF intensities for individual transitions separated widely in frequency, there is an unknown uncertainty in these measurements.

Although the rotational state distributions are nearly identical for all RH, the vibrational partitioning depends markedly on the type of C–H bond abstracted. Abstraction of primary hydrogens produces almost exclusively $v=0$ OH, abstraction of secondary hydrogens yields somewhat more $v=0$ than $v=1$, while abstraction of tertiary hydrogens yields slightly more $v=1$ than $v=0$ OH. It should be noted that only for the case of tertiary abstraction is a vibrational inversion achieved and chemical laser action possible.

Only at high collision energies are $v=2$ OH from $O(^3P) + (CH_3)_3CH$ and $v=2$ OD from $O(^3P) + C_6D_{12}$ energetically allowed. However, no signal was observed in either case and the limits $\sigma(v=2)/\sigma(v=1) \leq 10$ can be inferred for each. Unlike the rotational distributions, the vibrational state distributions do show a dependence on E_c. This is most accurately obtained from excitation functions and is shown later.

Classical trajectory calculations on model exothermic potential surfaces have shown that the vibrational state distribution in the products is sensitive to where the initial bond breaks during the course of the reaction, particularly for collinear surfaces.[8,13] If this occurs within the entrance channel, the surface is called attractive and produces much vibrational excitation in products. Conversely, if it occurs in the exit channel, the surface is labeled repulsive and little vibrational excitation occurs.

The results observed here for RH suggest the abstraction of primary hydrogens occurs on a repulsive surface, abstraction of secondary hydrogens on a more attractive surface, while abstraction of tertiary hydrogens is on an even more attractive surface. It is for this reason that the correlation diagrams were drawn shifted

TABLE I. Vibrational partitioning in the reactions $O(^3P) + RH \rightarrow OH(v) + R\cdot$ and $O(^3P) + RD \rightarrow OD(v) + R\cdot$.

Reactant	R–H bond[a]	E_c[b]	$\sigma(v=1)/\sigma(v=0)$
$C(CH_3)_4$	P	14.3	0.01
C_6H_{12}	S	7.1	0.24
$(CH_3)_3CH$	T	5.3	1.4
C_6D_{12}	S	7.5	0.7

[a] P, S, and T refer to primary, secondary, and tertiary hydrogens, respectively.
[b] Average center of mass collision energy in kcal/mole.

along Q relative to each other in Fig. 1. In essence, as this figure demonstrates, the more exothermic the reaction is in the homologous series and the lower the barrier, the more attractive is the surface. This generalization has been noted before.[18]

C. Fine structure partitioning

Spin–orbit interactions in the $^2\Pi$ radical OH causes a spin doubling and results in two manifolds of (v, K) levels split by ~ 125 cm^{-1}, the lowest corresponding to a $^2\Pi_{3/2}$ state and the higher to a $^2\Pi_{1/2}$ state.[19] In addition, each spin doublet is further split slightly by Λ doubling. These four fine structure states for each (v, K) level can be individually probed by different transitions in the $^2\Sigma - ^2\Pi$ band.[10] A comparison between the intensities of these various transitions yields the partitioning into the fine structure levels.

Previous measurements on the reactions $H + NO_2 \rightarrow OH + NO$[20] and $O(^1D_2) + H_2 \rightarrow OH + H$[21,28] have demonstrated a strong selectivity in Λ-doublet components for high K levels, but no selectivity in the spin doublets. The selectivity in Λ doublets was explained in terms of a preferentially bent but planar geometry for reaction. In contrast to these cases, the reaction of $O(^3P) + RH$ has no selectivity in Λ-doublet components, but does show a preference in the spin doublets as shown in Fig. 6. It can be seen that for this reaction the $\Pi_{3/2}$ levels of OH are nearly twice as populated as $\Pi_{1/2}$. Similar results were observed for all other RH reactants as well. OD produced from the reaction $O(^3P) + C_6D_{12}$ yields ~ 1.4 times as much $\Pi_{3/2}$ as $\Pi_{1/2}$.

Only very low rotational states of OH are populated in these reactions. However, it is only for high K states that Λ-doublet components can be uniquely associated with directed orbitals[22] and produce a selectivity. Thus, it is not surprising that the $O(^3P) + RH$ reactions produce

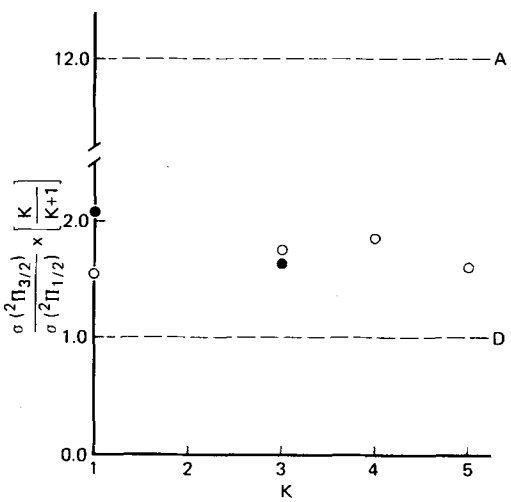

FIG. 6. Partitioning into the OH spin doublets in the reaction $O(^3P) + C_6H_{12} \rightarrow OH + C_6H_{11}$. K is the rotational quantum number and the ordinate is the ratio of spin doublets, corrected for the different $2J+1$ degeneracy. The dashed line labeled D represents the diabatic scattering limit while that labeled A is the adiabatic scattering limit. The ● are for OH ($v = 1$) and o for OH ($v = 0$) states.

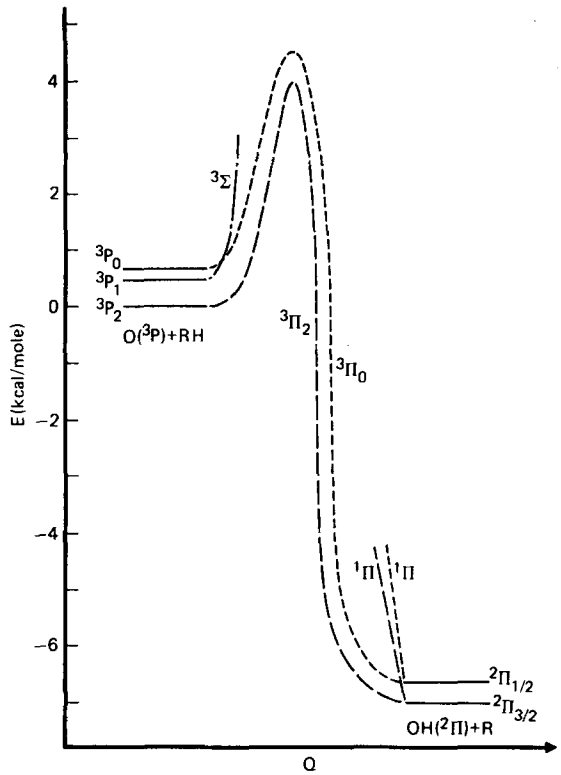

FIG. 7. Schematic correlation diagram for the reaction $O(^3P) + RH \rightarrow OH + R\cdot$ including the spin–orbit surfaces and assuming $C_{\infty v}$ symmetry. E is the energy and Q is the reaction coordinate. The labels on the left are the spin–orbit states of $O(^3P)$ and on the right are the labels of the spin doublets of $OH(^2\Pi)$.

both Λ-doublet components equally.

It is unlikely that spin states are selected by the reactive collision since this would require a strong magnetic coupling during the scattering. However, inspection of the adiabatic correlation diagram for the reaction including all spin–orbit levels (Fig. 7) does provide a possible explanation in terms of the initial $O(^3P)$ spin–orbit states. This diagram is constructed assuming linear reaction symmetry and treating the R· as a spherical particle. The correlations are drawn from the fact that the vector sum of spin and orbital momentum, the total angular momentum, must be conserved in the adiabatic limit. $O(^3P_2)$ correlates with $OH(^2\Pi_{3/2})$ through a $^3\Pi_2$ surface, $O(^3P_0)$ connects to $OH(^2\Pi_{1/2})$ through a $^3\Pi_0$ surface, while $O(^3P_1)$ does not correlate with $OH(^2\Pi)$ at all, but rather with a nonreactive $^3\Sigma$ surface.

Although the O_2 discharge produces $O(^3P)$ in an unknown, but presumably hot, distribution of spin–orbit states, the flow subsequent to dissociation in the atom source cools this distribution substantially. EPR experiments[23] have demonstrated that the spin–orbit states of $O(^3P)$ are efficiently relaxed in such flows, and we anticipate the distribution to by nearly thermal at ~ 300°K, similar to translation. Under these conditions, the $O(^3P)$ beam composition is $\sim 72\%$ $^3P_2$, $\sim 22\%$ $^3P_1$, and $\sim 6\%$ $^3P_0$.

If the reaction is strictly adiabatic, i.e., there are

no transitions between the surfaces caused by the collision, and the reactive cross sections are similar on the $^3\Pi_2$ and $^3\Pi_0$ surfaces, then we expect to produce OH with the distribution $\sigma(^2\Pi_{3/2})/\sigma(^2\Pi_{1/2})\times[K/K+1]=12$. On the other hand, if the reaction is completely diabatic, there are many transitions between the surfaces during the course of the collision. Then there is no memory of the initial distribution in the O(^3P) spin–orbit states, and we always expect an OH distribution $\sigma(^2\Pi_{3/2})/\sigma(^2\Pi_{1/2})\times[K/K+1]=1$. Our result $\sigma(^2\Pi_{3/2})/\sigma(^2\Pi_{1/2})\times[K/K+1]\approx 2$ is midway between these two limits. We conclude that these reactions are neither fully in the adiabatic nor diabatic limit, but that partial collisional mixing of the surfaces occurs.

IV. EXCITATION FUNCTIONS

Excitation functions have been measured for the ground rotational level in each vibrational state of the various RH reactants. These excitation functions represent the variation of the individual cross sections $\sigma(v, K=1, f_1')$ with the average initial center of mass collision energy E_c. In contrast to the state distributions which were obtained by scanning the laser at fixed E_c, the excitation functions are obtained when the laser is held at a fixed frequency on top of the $Q_1(v, K=1)$ transition and the LIF intensity is monitored as E_c is varied.

E_c is varied by changing the velocity of the seeded RH nozzle beam. A range of velocities are obtained from a given gas mixture by heating the nozzle tip from ~300 to 800°K. These velocity ranges are shifted somewhat by changing either the relative concentration of RH in the seeded gas mixture or the carrier gas identity, i.e., H_2 or He. In regions of overlap between the ranges of RH velocity, good agreement was obtained for the excitation functions. Since the population of internal modes in RH, especially rotation and low frequency vibration, should be dramatically affected by the different nozzle conditions, it is concluded that the changes in LIF intensity arise from variations in E_c, and thus represents the translational excitation function.

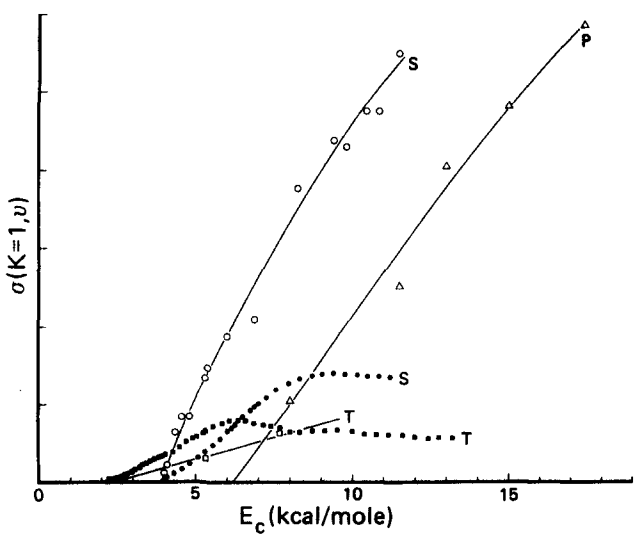

FIG. 8. Excitation functions for the reactions O(^3P) + RH → OH + R·. The ordinate is the relative cross section and E_c is the average center of mass collision energy. The curves labeled T are for reaction with $(CH_3)_3CH$ to produce OH ($K=1, v=1$) (■) and OH ($K=1, v=0$) (□), those labeled S are for C_6H_{12} to produce OH ($K=1, v=1$) (●) and OH ($K=1, v=0$) (○), and the one labeled P is for $(CH_3)_4C$ to produce OH ($K=1, v=0$) (△).

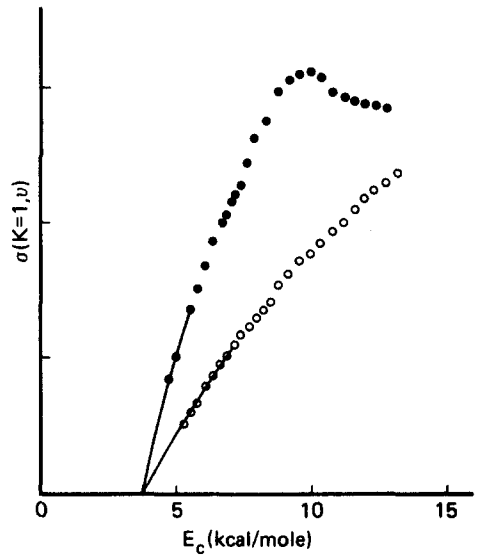

FIG. 9. Excitation function for the reaction O(^3P) + C_6D_{12} → OD + C_6D_{11}. The ordinate is the relative cross section and E_c is the average center of mass collision energy. The (●) are for OD ($K=1, v=1$) and the (○) are for OD ($K=1, v=0$).

As before, cross sections were obtained from Eq. (2). Since n_{RH} varies with nozzle conditions, i.e., gas composition and nozzle temperature, relative values of n_{RH} were measured separately for each E_c using modulated beam mass spectrometry. Excitation functions for different RH species were scaled to each other by comparing LIF intensities at fixed E_c and known RH densities in the nozzle. Normalization of the $v=0$ to $v=1$ excitation functions for a given RH was obtained from the measurements of vibrational partitioning described earlier. Since it has been demonstrated that there is little variation in rotational or fine structure distribution with E_c, the results for the $(K=1, v)$ level are characteristic for the entire vibrational state.

The results for such measurements for different RH are given in Fig. 8 and for the analogous states of OD from the reaction O(^3P) + C_6D_{12} in Fig. 9. These figures demonstrate very nicely the threshold behavior for the abstraction reactions. The E_c scale is calculated from TOF measurements on the seeded nozzle and O(^3P) beams. The open symbols represent excitation functions for the $(K=1, v=0)$ levels while the solid symbols are for the $(K=1, v=1)$ levels. Because of the OH background in $v=0$, there is considerably more noise associated with the $(K=1, v=0)$ excitation functions. The two data points in Fig. 8 for the excitation function of $v=0$ $(CH_3)_3CH$ were not obtained by the experimental procedures outlined above. They were calculated from the $v=1$ excitation function and the measurements of vibrational partitioning at the two E_c.

The dynamic thresholds for reaction E_0 are obtained approximately for each RH when the energy distribution

TABLE II. Comparisons of dynamic thresholds (kcal/mole) and activation energies (kcal/mole) obtained from thermal rate constants.

Reactant	E_0	E_A (rate constant)
$C(CH_3)_4$	6.2	5.8[a]
C_6H_{12}	4.5	4.4[b]
$(CH_3)_3CH$	3.0	3.3[c]

[a]Reference 5.
[b]P. Kim and R. B. Timmons, Int. J. Chem. Kinet. 7, 143 (1975).
[c]Value taken from 2,3-dimethylbutane which has two rather than one tertiary hydrogen; Ref. 5.

of E_c is deconvoluted. This is accomplished by assuming a linear post threshold dependence of the cross sections $\sigma \sim (E_c - E_0)$ and Monte Carlo integration over the experimental parameters which define the energy distribution, i.e., the spread in initial velocities and angles for both beams. It should be pointed out that at low E_c (~5 kcal/mole), the energy resolution $\delta E/E \approx 0.35$ is rather poor due to both the angular and velocity spread in the $O(^3P)$ beam. At higher E_c (~15 kcal/mole), $\delta E/E \approx 0.25$ and is somewhat better.

As these figures indicate, no reaction occurs until a definite energetic threshold is reached for each RH, and then the cross section rises nearly linearly with E_c. For C_6H_{12} and C_6D_{12} reactants, the excitation functions for both $v=0$ and $v=1$ OH (OD) yield the same dynamic threshold. This demonstrates that both the $v=0$ and $v=1$ vibrational states are below the potential barrier.

Although dynamic thresholds are not exactly equivalent to activation energies, they are closely related.[24] There is good agreement between the dynamic thresholds and activation energies obtained from thermal rate constants, as shown in Table II. It should be pointed out that while $(CH_3)_3CH$ has several primary and only one tertiary hydrogen, the low threshold and shape of the excitation function is characteristic for abstraction of only the tertiary hydrogen. This was confirmed by experiments on $(CH_3)_3CD$ as the reactant at modest E_c, since only the product OD was observed. Unfortunately, the thresholds could not be determined accurately enough to measure the small isotope shift in the threshold between the reactions $O(^3P) + C_6H_{12}$ and $O(^3P) + C_6D_{12}$.

The initial slopes of the total reaction excitation functions are related to the pre-exponential factors in the Arrhenius form of the thermal rate constants.[24] Although absolute values of these pre-exponential factors cannot be determined, comparison between the different RH is possible. From our measurements, we calculate values of $A_p : A_s : A_T \equiv 0.6 : 1.0 : 1.7$, where A_p, A_s, and A_T are the relative pre-exponential factors per hydrogen atom for primary, secondary, and tertiary hydrogens, respectively. The values obtained from thermal rate constants are $A_p : A_s : A_T \equiv 0.5 : 1.2 : 1.6$.[5] Thus, both the thresholds and relative slopes obtained from the excitation functions are consistent with thermal rate constant measurements.

The most striking feature in the excitation functions is that although the $v=0$ curves continue to increase smoothly with E_c, the $v=1$ excitations abruptly cease rising ~3–4 kcal/mole above threshold and in fact decrease somewhat. This is particularly apparent in Fig. 9, although the actual shapes for the $v=1$ OD from C_6D_{12} and $v=1$ OH from C_6H_{12} are quite similar. The immediate implication is that vibrational partitioning into OH decreases at higher E_c.

The abrupt change in the $v=1$ OH slope suggests that another product channel may become active that competes with $v=1$ OH formation but not $v=0$ OH formation. However, this change does not occur at any known thermodynamic threshold. The most likely explanation is that vibrational excitation into the R· fragment becomes allowed at sufficiently large E_c. If there is a strong coupling between vibrations in the R–H–O transition state, then excitation of R· modes can only occur at the expense of OH vibration. Although the identity of the exact R· modes which are important is impossible to determine due to the large number of such modes, it seems probable that C–C stretches, C–C–C bends and C–C–H bends are involved. This tentative explanation infers that there is little vibrational excitation in R· at E_c below this sharp bend over.

V. CONCLUSIONS

The molecular beam measurements reported here for the reactions of $O(^3P)$ with many different saturated hydrocarbons have confirmed the identity of OH as the primary product and the abstraction mechanism [Eq. (1)]. The dynamic thresholds for OH formation are in good agreement with activation energies obtained from thermal rate constants. This demonstrates that the rate limiting step in the $O(^3P) + RH$ reactions is this abstraction process.

The general picture that emerges is that these reactions are dominated by interactions of $O(^3P)$ with the individual C–H bonds. This suggests, at least qualitatively, that R· may be considered a structureless particle, i.e., that a triatomic model is appropriate to describe most features of the dynamics of these reactions. A variety of evidence suggests this generalization. Firstly, the OH rotational state distributions imply that reaction only occurs when $O(^3P)$ is collinear to a C–H bond. Further, this rotational distribution is nearly independent of the complexity or nature of the hydrocarbon. Secondly, the shape of the excitation functions suggests that little vibrational excitation of R· internal modes occur at low E_c. Thirdly, the triatomic model is also consistent with the approximate bond additivity of the thermal rate constants. It is demonstrated in the following paper that this triatomic model quantitatively describes nearly all features of the dynamics of the $O(^3P) + RH$ reactions.

The measurements reported here provide many qualitative features of the R–H–O potential surfaces. The small excitation of OH rotation implies a very collinear reactive surface, typically $\leq 15°$ with respect to the R–H bond. This collinearity in the surface is quite general for all RH, and explains the small pre-exponential

factors observed in the thermal rate constants. The observed collinear interaction is consistent with recent *ab initio* and scattering calculations on the $O(^3P) + H_2$ potential surface.[25,26] This surface should be qualitatively similar to the $O(^3P) + RH$ triatomic surface.

The measurements of vibrational partitioning into OH provide information as to where the R–H bond breaks during the course of the reaction. This point shifts from the exit towards the entrance valley along the series for primary, secondary, and tertiary abstraction.

The observed dynamic thresholds yield the height of the potential barrier when corrections for vibrational zero point energy are included.

The measurements of OH fine structure partitioning demonstrate that the $O(^3P) + RH$ reactions are partially adiabatic with respect to the spin–orbit surfaces. Approximate semiclassical calculations on the reaction $F(^2P_{3/2,1/2}) + H_2$ also indicate only partial mixing of spin–orbit surfaces in this reaction as well.[27] These FH_2 surfaces, however, are nearly degenerate only in the asymptotic entrance channel rather than along the entire surface as for OHR.

There is no evidence from our measurements that triplet to singlet surface crossings play any role in the reactions since all state distributions are consistant with the direct abstraction process on the triplet surface. There is evidence, however, that these crossings are important for the analogous reactions initiated on the singlet surface.[28]

These qualitative features of the potential surfaces and dynamics are discussed more quantitatively in the following paper.[13] There, we report quasiclassical trajectory calculations on semiempirical LEPS potential surfaces, and assume a triatomic model for the R–H–O interaction. These results indicate that a single interaction potential yields excellent agreement with the experimental results reported here.

VI. ACKNOWLEDGMENTS

The authors gratefully acknowledge the technical assistance of V. T. Maxson in all phases of the experiments, D. Horne for the design and construction of all critical electronics, and R. K. Nesbet, R. Schinke, and B. Liu for many useful discussions.

[1] J. T. Herron and R. E. Huie, J. Phys. Chem. Ref. Data 2, 467 (1973).
[2] G. Paraskevopoulos and R. J. Cvetanović, J. Phys. Chem. 81, 2598 (1977).
[3] R. F. W. Bader and R. A. Gangi, J. Am. Chem. Soc. 93, 1831 (1971).
[4] D. Golden and S. Benson, Chem. Rev. 69, 125 (1969).
[5] J. T. Herron and R. E. Huie, J. Phys. Chem. 73, 3327 (1969).
[6] R. D. Levine and R. B. Bernstein, *Molecular Reaction Dynamics* (Oxford University, New York, 1974).
[7] N. H. Hijazi and J. C. Polanyi, Chem. Phys. 11, 1 (1975).
[8] J. C. Polanyi, Acc. Chem. Res. 5, 161 (1972).
[9] For a review, see R. N. Zare and P. J. Dagdigian, Science 185, 739 (1974).
[10] H. M. Crosswhite and G. H. Dieke, J. Quant. Spectrosc. Radiat. Transfer 2, 97 (1962). Unless otherwise noted, the OH spectroscopic notation used throughout this paper is that of Ref. 10.
[11] R. P. Mariella, Jr., B. Lantzsch, V. T. Maxson, and A. C. Luntz, J. Chem. Phys. 69, 5411 (1978).
[12] B. Liu (private communication).
[13] A. C. Luntz and P. Andresen, J. Chem. Phys. 72, 5851 (1980) (following paper).
[14] S. N. Foner and R. L. Hudson, J. Chem. Phys. 25, 1680 (1959).
[15] R. L. Brown, J. Phys. Chem. 71, 2492 (1967).
[16] F. Kaufman, in *Progress in Reaction Kinetics*, edited by G. Porter (Pergamon, New York, 1961), Vol. 1, p. 13.
[17] H. Pauly and P. Toennies, in *Methods of Experimental Physics*, edited by B. Bederson and W. L. Fife (Academic, New York, 1968), Vol. 7A, p. 227.
[18] M. H. Mok and J. C. Polanyi, J. Chem. Phys. 51, 1451 (1969).
[19] For low K states, notation corresponding to Hund's coupling case a is more appropriate to describe the fine structure levels.
[20] R. P. Mariella, Jr. and A. C. Luntz, J. Chem. Phys. 67, 5398 (1977).
[21] A. C. Luntz, R. Schinke, V. T. Maxson, and Hs. Günthard (to be published).
[22] W. D. Gwinn, B. E. Turner, W. Miller Goss, and G. L. Blackman, Astrophys. J. 179, 789 (1973).
[23] S. Krongelb and M. W. P. Strandberg, J. Chem. Phys. 31, 1196 (1959).
[24] M. Menzinger and R. Wolfgang, Angew. Chem. 8, 438 (1969).
[25] R. E. Howard, A. D. McLean, and W. A. Lester, Jr., J. Chem. Phys. 71, 2412 (1979).
[26] R. Schinke and W. A. Lester, Jr., J. Chem. Phys. 70, 4893 (1979).
[27] J. C. Tully, J. Chem. Phys. 60, 3042 (1974).
[28] A. C. Luntz, J. Chem. Phys. (in press).